0090-9556/08/3603-571–581$20.00
DRUG METABOLISM AND DISPOSITION
Vol. 36, No. 3
17954/3311231
Printed in U.S.A.

DMD 36:571–581, 2008

Aryl-Propionamide-Derived Selective Androgen Receptor Modulators: Liquid Chromatography-Tandem Mass Spectrometry Characterization of the in Vitro Synthesized Metabolites for Doping Control Purposes

Tiia Kuuranne, Antti Leinonen, Wilhelm Schänzer, Matthias Kamber, Risto Kostiainen, and Mario Thevis

Institute of Biochemistry—Center for Preventive Doping Research, German Sports University Cologne, Cologne, Germany (T.K., W.S., M.T.); Doping Control Laboratory, United Laboratories Ltd., Helsinki, Finland (T.K., A.L.); Department of Doping Prevention, Federal Office of Sports, Magglingen, Switzerland (M.K.); and Division of Pharmaceutical Chemistry, Faculty of Pharmacy, University of Helsinki, Helsinki, Finland (R.K.)

Received August 8, 2007; accepted December 17, 2007

ABSTRACT:

Selective androgen receptor modulators (SARM) are a prominent group of compounds for being misused in sports owing to their advantageous anabolic properties and reduced side effects. To target the preventive doping control analysis in relevant compounds, the challenge is to predict the metabolic fate of a new compound. For aryl-propionamide-derived SARM, an in vitro assay employing microsomal and S9 human liver enzymes was developed to simulate phase-I and phase-II metabolic reactions. In vitro metabolic profiles and the structure-metabolic relationship were compared between four structurally modified substrates. Accurate mass measurements were used to characterize the synthesized metabolites, and also collision-induced dissociation was examined to suggest the methodological approach to monitor the prohibited use of aryl-propionamide-derived drug candidates. Subsequent phase-I and phase-II metabolic reactions were successfully combined in one in vitro assay. The main routes of phase-I modifications involved the hydrolysis of ether linkage, monohydroxylation, and hydrolytic cleavage of the amide bond. Nitro-reduction and deacetylation were reactions observed for substrates possessing the corresponding functionality. SARM metabolites were analyzed in negative ion electrospray ionization and detected as deprotonated species $[M-H]^-$. The main metabolic modifications were observed to occur in the B-ring side, and collision-induced dissociation resulted in the product ions originating from the A-ring side of the compound. These structure-specific ions may be monitored as target ions in the routine doping control.

For decades, steroidal androgens have been clinically used in the treatment of diseases related to androgen deficiency, including muscle-wasting, osteoporosis, and benign prostate hyperplasia, but recently their suitability for hormone replacement therapy of aging men and regulation of male fertility has been under investigation (Negro-Vilar, 1999; Gao and Dalton, 2007). Traditional anabolic-androgenic therapies, applying steroid-structured compounds such as testosterone, are often limited due to low oral bioavailability, cross-reactivity with steroid receptors other than the androgen receptor, hepatic toxicity, and other undesirable side effects on the prostate and cardiovascular system (Bhasin and Bremner, 1997). To overcome these drawbacks, a series of nonsteroidal selective androgen receptor modulators (SARM) have been developed. SARM represent enhanced tissue selectivity, binding to the androgen receptor (AR) with affinity similar to testosterone, but exhibiting only partial agonist properties in androgenic tissue. Based on their chemical structure, most prominent pharmacophores of SARM can be categorized at least in four classes: 1) aryl-propionamide, 2) bicyclic hydantoin, 3) quinoline, and 4) tetrahydroquinoline analogs, which all have also entered different stages of clinical studies (Chen et al., 2005a; Thevis and Schänzer, 2007). Among the published data on SARM research, the series of aryl-propionamide-derived analogs are the most widely described (Brown, 2004; Chen et al., 2005a; Mohler et al., 2005).

In the development of new aryl-propionamide-derived SARM with higher pharmacological activity, better selectivity, and more advantageous pharmacokinetic properties, several structure-activity and in vitro and in vivo metabolic studies have been carried out (Kirkovsky et al., 2000; Chen et al., 2005b; Gao et al., 2006; Wu et al., 2006). The principal structure of aryl-propionamide-derived SARM consists of *para*-substituted phenol residue linked to a 2-hydroxy-2-methylpropionamide functionality bearing a bi-substituted phenyl group (Table 1). A modification to replace the thioether function of the very first

We thank the Manfred Donike Institute for Doping Analysis, Cologne, and the Federal Office of Sports, Switzerland, for supporting the presented work.

Article, publication date, and citation information can be found at http://dmd.aspetjournals.org.

doi:10.1124/dmd.107.017954.

ABBREVIATIONS: SARM, selective androgen receptor modulator(s); ACN, acetonitrile; AR, androgen receptor; CID, collision-induced dissociation; ESI, electrospray ionization; LC, liquid chromatography; MS, mass spectrometry; MS/MS, tandem mass spectrometry; PAPS, adenosine 3′-phosphate 5′-phosphosulphate; TFA, trifluoroacetic acid; UDPGA, uridine 5′-diphosphoglucuronic acid; amu, atomic mass unit(s).

TABLE 1

Abbreviations, nomenclature, and structures of the aryl-propionamide-derived SARM of the study (S1-S4) and the androgen receptor agonist bicalutamide

Abbreviation	Compound	Structure
	Bicalutamide	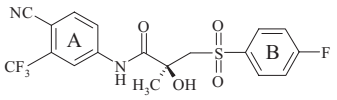
S1	3-(4-Fluorophenoxy)-2-hydroxy-2-methyl-N-[4-cyano-3-(trifluoromethyl)phenyl]-propanamide	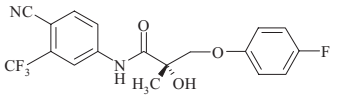
S2	3-(4-Fluorophenoxy)-2-hydroxy-2-methyl-N-[4-nitro-3-(trifluoromethyl)phenyl]-propanamide	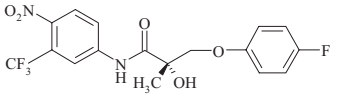
S3	3-(4-Chlorophenoxy)-2-hydroxy-2-methyl-N-[4-nitro-3-(trifluoromethyl)phenyl]-propanamide	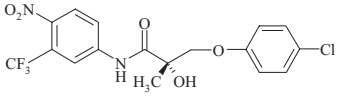
S4	3-(4-Acetylamino-phenoxy)-2-hydroxy-2-methyl-N-[4-nitro-3-(trifluoromethyl)phenyl]-propanamide	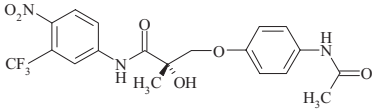

pure AR antagonist, bicalutamide, by an ether linkage was found to result in better metabolic stability and, thus, increased the in vivo half-life and pharmacological activity of the drug candidates (Marhefka et al., 2004). An electron-withdrawing function in position 4 of the A-ring was reported to be advantageous for AR-binding of the substrate, mimicking the AR interaction of the steroidal 3-keto-function (Bohl et al., 2004), and the more electronegative 4-nitro-function favored the binding over cyano-function. However, a nitro group increases the metabolic reactivity of the substrate, which is suggested to contribute greatly to the in vivo clearance of the compound and also to have an effect on the amide hydrolysis and, thus, on the enhanced metabolism of the analogs (Wu et al., 2006). With respect to B-ring substitution, *para*-substituted ligands were reported to bind to AR with higher affinities than the corresponding *meta*-substituted analogs of bicalutamide derivatives (Kirkovsky et al., 2000).

When considering the pharmacological activity of the candidate molecules, metabolic reactions, especially those producing active metabolites, are of major interest, in which the hepatic enzyme activity plays a significant role. According to earlier studies, the major metabolites of aryl-propionamide-derived SARM, depending on the initial substrate structure, arise from nitro-reduction, hydroxylation, acetylation, and hydrolytic reactions (Gao et al., 2006; Wu et al., 2006) involving both cytosolic and microsomal enzymes. From the doping control point of view, the main interest of the metabolic studies is, however, to characterize the main metabolites and their physicochemical properties in order to include target compounds in the routine screening procedures.

As a prominent new group of compounds for being misused in sports due to advantageous anabolic properties and reduced side effects (Gao et al., 2005), the methods to detect the potential use of SARM are of the utmost importance in preventive doping control. As demonstrated earlier (Catlin et al., 2002; Catlin et al., 2004, Sekera et al., 2005), doping control laboratories should be prepared to measure also pharmacologically attractive compounds, which do not have clinical approval to enter the market.

To predict the metabolic reactions of aryl-propionamide-derived SARM, an in vitro assay was developed to simulate phase-I and phase-II metabolic reactions. Fractions of microsomal and S9 human liver preparations were used as sources of metabolizing enzymes, and the cosubstrates of the synthesis mixture were selected to allow phase-I metabolic reactions, followed by phase-II glucuronidation and sulfonation. In addition to comparing the in vitro metabolic profiles and structure-metabolic relationship of four structurally modified substrates, electrospray ionization (ESI) and collision-induced dissociation (CID) of the synthesized metabolites were examined in order to suggest the methodological approach for the monitoring of the prohibited use of aryl-propionamide-derived drug candidates for doping control purposes.

Materials and Methods

NADPH was purchased from Roche Diagnostics (Mannheim, Germany), adenosine 3′-phosphate 5′-phosphosulphate (PAPS) from Calbiochem/EMD Biosciences Inc. (La Jolla, CA), and D-saccharic acid 1,4-lactone and uridine 5′-diphosphoglucuronic acid (UDPGA) from Sigma (St. Louis, MA). High-performance liquid chromatography grade solvents and analytical or higher grade reagents were used throughout the study.

Synthesis of Aryl-Propionamide-Derived SARM. All the substrates for the in vitro assays were prepared via established chemical synthesis procedures (Tucker et al., 1988; Tucker and Chesterson, 1988; Marhefka et al., 2004), and the characterization of the synthesis products is published and discussed earlier in detail (Thevis et al., 2006). The SARM of this study are listed in Table 1.

Enzymatic Protein. Human liver microsomal and S9 fractions were purchased from BD Gentest (Woburn, MA), and both preparations presented pooled mixtures of different individual donors.

In Vitro Metabolic Assays. Stock solutions (10, 50, and 100 μM) of each tested substrate for in vitro metabolic activity were prepared in dimethyl sulfoxide. For initial experiments, reaction mixtures were prepared in 50 mM phosphate buffer (pH 7.4) containing 5 mM $MgCl_2$ at substrate concentrations of 0, 1, 5, and 10 μM and 5 mM NADPH. One sample containing all reaction components but the enzymatic protein was also added to the batch to monitor the potential nonenzymatic reactions within the incubation period. To those samples, which were subjected to glucuronidation, D-saccharic acid 1,4-lactone

(5 mM) was added as glucuronidase inhibitor. The reaction was initiated by adding the appropriate enzymatic protein (20 μg/incubation), and the phase-I reaction was run in an incubation volume of 100 μl for 120 min at 37°C. For the subsequent phase-II reaction step, either UDPGA (5 mM) or PAPS (20 μM) was added to the mixture for glucuronidation or sulfonation, respectively, and carried out for 120 min at 37°C. The overall reaction was terminated by the addition of 100 μl of ice-cold acetonitrile (ACN) and transferred to ice. The reaction mixtures were then centrifuged (6000*g*, 10 min), and acetonitrile was evaporated from the supernatants in vacuo before further sample purification.

Liquid-Liquid Extraction. Aqueous phase was acidified by adding 20 μl of acetic acid (2%); the supernatants were extracted twice with 500 μl of ethyl acetate, and organic layers were combined and evaporated to dryness in vacuo. Dry residues were dissolved in 50 μl of the liquid chromatographic eluent mixture A/B (9:1, see *Liquid Chromatography-Mass Spectrometry* for details).

Liquid Chromatography-Mass Spectrometry. LC-ESI-MS(/MS) of the in vitro synthesized SARM metabolites was performed on an instrument setup consisting of an Agilent 1100 Series high-performance liquid chromatography system (Agilent Technologies, Waldbronn, Germany) and an Applied Biosystems 4000 Q Trap mass spectrometer (Applied Biosystems, Darmstadt, Germany). The LC system was equipped with a Waters (Milford, MA) XTerra RP_{18} Isis column (2.1 $\times$ 150 mm; particle size, 3.5 μm), and the eluents used were 5 mM ammonium acetate with 0.1% acetic acid (eluent A) and acetonitrile (eluent B). The gradient run started with an isocratic step (A/B, 9:1) of 3 min. The acetonitrile gradient was then ramped from 10% to 100% in 12 min and held at 100% for 8 min, and finally the system was equilibrated for 5 min. The flow rate was 250 μl/min, and the injection volume was 5 μl. The analyses were carried out in negative ion mode ESI applying the ion spray voltage of -4200 V and source temperature of 500°C. For the initial screening of the metabolites, *m/z* range 200 to 700 was analyzed, and for the identification of the metabolites, the MS/MS collision offset voltage was selected to preserve approximately 10% of the precursor ion. Nitrogen was used as collision gas (6.0×10^{-3} Pa). This method was used for the screening of the in vitro assay samples, and for the initial fragmentation studies, as well as for the determination of the relative abundance of the metabolites using Analyst 1.4.2 software (Applied Biosystems). Relative abundance of each metabolite was calculated from the basis of the absolute peak height from an extracted ion chromatogram of the ion transition using 0.5 amu resolution as the extraction criterion.

High Resolution-High Accuracy Experiments. LC-ESI-MS(/MS) for the high-resolution/high-accuracy determination of the elemental composition SARM metabolites and the main product ions was performed on a Thermo LTQ Orbitrap mass spectrometer (Thermo Fisher Scientific, Bremen, Germany) combined with an Agilent 1100 Series HPLC system with isocratic pump (pump 1) and capillary pump (pump 2). The trapping column employed was an Agilent Zorbax 300SB-C18 (2 $\times$ 0.3 mm; particle size, 3.5 μm), and the main analytical column was a Zorbax 300SB-C18 (50 $\times$ 0.3 mm; particle size, 3.5 μm). The mobile phase for pump 1 was ACN/aqueous solution of 0.1% acetic acid and 0.01% TFA (3/97) with an isocratic flow rate of 50 μl/min. For pump 2, eluents A (aqueous solution of 0.1% acetic acid and 0.01% TFA) and B (ACN/aqueous solution of 0.1% acetic acid and 0.01% TFA; 4:1) were used with a primary flow rate of 200 μl/min, which was further split to a microflow of 10 μl/min and directed to the ESI source. The gradient run started with an isocratic step (A/B, 95:1) of 2 min, followed by a linear ramp of B from 5 to 40% in 18 min, and further from 40 to 97% in 14 min. These conditions were held for 10 min, and then the column was equilibrated for 16 min in the initial conditions of the run. Injection volume was 5 μl, and the column oven was maintained in 30°C throughout the analysis. The Orbitrap was operated in negative ion ESI mode and calibrated using the calibration mixture suggested by the manufacturer (LTQ Orbitrap calibration solution). The ionization voltage was -3100 V, and the capillary temperature was set to 275°C. The damping gas in the linear ion trap was helium (purity, 5.0), and the gas for the curved linear ion trap was nitrogen from a CMC nitrogen generator (CMC Instruments, Eschborn, Germany).

Results

In Vitro Assay and Metabolic Reactions of Aryl-Propionamide-Derived SARM. Simulations of in vitro metabolism of the four SARM substrates were carried out in an assay consisting of the cosubstrates (NADPH, UDPGA, and PAPS) and enzymes (microsomal and S9 fractions of human liver tissue preparations) for subsequent phase-I and phase-II reactions in one assay. For compound S1, the major in vitro metabolic route was the hydrolysis of the ether linkage, that is, "*O*-dephenylation," which cleaved the B-ring (M11; Fig. 1 and Table 2), presumably initiated by an oxidation of the carbon atom adjacent to the *O*-phenyl residue. A subsequent elimination of 4-hydroxy acetanilide may yield an aldehyde of the remaining propionanilide that undergoes reduction to the metabolic product M11. Alternatively, a hydroxylation of the phenyl residue *ortho*-positioned to the substituent could trigger the dephenylation via a mechanism described in a metabolism study on the nontricyclic antidepressant nefazodone (Kalgutkar et al., 2005). The other main metabolic route was monohydroxylation, which resulted in the formation of two different metabolites (M3). Both metabolites were presumably also further conjugated with glucuronic acid (M5). Sulfonation of the monohydroxylated metabolite (M4), however, was observed to result only in one metabolite. Although the CID pattern (Table 3) indicates that the main site of monohydroxylation is the B-ring, it is also occurring on the A-ring, at least to some extent, as the metabolite originating from monohydroxylation and hydrolytic cleavage of the amide bond (M12) was also detected (Table 2). This metabolite, however, was only minor, and readily sulfonated (M13) and glucuronidated (M14) in further phase-II reactions. Substrate S1 was found to directly sulfonate (M1) and conjugate to glucuronic acid (M2), with closely similar relative activities.

Similarly to S1, compound S2 exhibited *O*-dephenylation (M11) and monohydroxylation (M3) as the two major metabolic pathways, from which the latter with three individual metabolites was the most dominating reaction (Fig. 1 and Table 2). Again, these three monohydroxylated compounds were also found as glucuronide-conjugates (M5), whereas only one sulfonated species (M4) was detected, and also with relative intensity clearly lower than those of M5-metabolites. Amide hydrolysis, combined with monohydroxylation and phase-II reactions, led to the formation of metabolites M13 and M14, from which sulfonation (M13) was dominating over glucuronidation (M14). Reduction of the nitro-group (M7) corresponded to 5% of the total in vitro metabolism of S2, and in comparison to other substrates, formation of a nitro-reduced and dihydroxylated metabolite was exceptionally observed both as free (M8) and glucuronide-conjugated (M9) compound (Fig. 1 and Table 2). According to the earlier results by Wu et al. (2006), dihydroxylation is suggested to occur in the B-ring, with which the results of this in vitro assay are in good agreement. Substrate S2 was found to undergo direct phase-II reactions, from which glucuronidation (M2) clearly dominated over sulfonation (M1) activity.

Among the selected aryl-propionamide-derived SARM within this study, in vitro metabolism of S3 showed an exceptional pattern, as *O*-dephenylation (M11) corresponded to more than 70% of the total observed metabolism, and all the other reaction types were only $\leq$6% in relative abundance (Fig. 1 and Table 2). From these reactions, the hydrolysis of the amide bond combined with monohydroxylation and glucuronide-conjugation (M14) was predominant, together with the second hydrolytic reaction and monohydroxylation, which led to the formation of monohydroxylated *N*-(4-nitro-trifluoromethyl-phenyl)-acetamide (M17). Three monohydroxylated metabolites were observed (M3), as well as the corresponding three glucuronide-conjugates (M5) and one sulfonated metabolite (M4) of S3. Minor metabolites resulted also from dehydroxylation (M6) and nitro-reduction (M7). Direct sulfonation (M1) and glucuronidation (M2) of

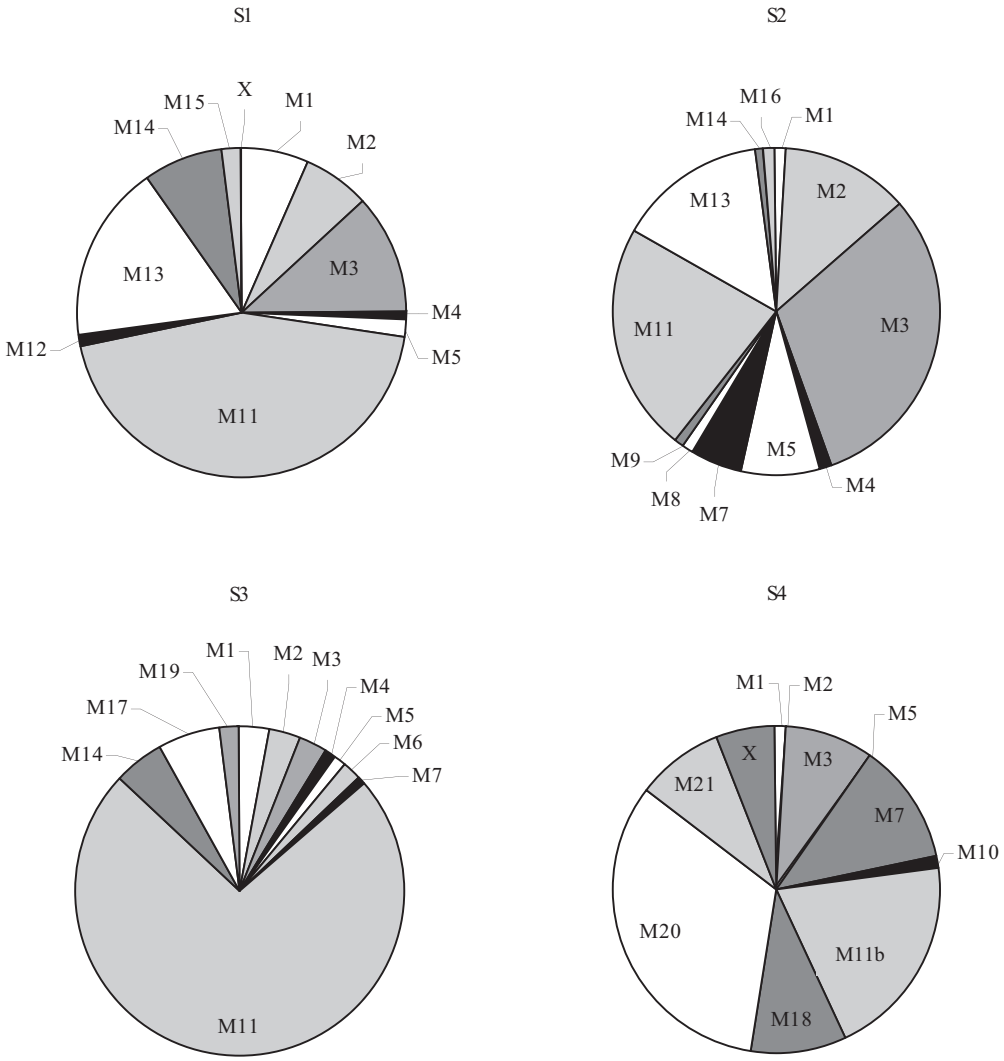

FIG. 1. Relative abundance of the detected metabolites from compounds S1, S2, S3, and S4. See Table 2 for more information on metabolites.

S3 was also observed, with relative abundance of these two conjugates being approximately equal.

Acetylamino *para*-substitution of the B-ring was strongly involved in the metabolic reactions of substrate S4 (Fig. 1 and Table 2). The main in vitro metabolite (M20) was detected in negative ion mode ESI at ion transition *m/z* 397 and the other (M21), exhibiting the relative abundance of 9% of the total metabolism, at *m/z* 478, both with retention times indicating less polar chemical properties than S4. Based on the Orbitrap accurate mass measurements (Table 4) and MS/MS structure characterization (Table 3), an elemental composition of $C_{17}H_{12}O_6N_2F_3$ was determined for M20 and $C_{22}H_{19}O_6N_2F_3$ for M21. The modifications, that is, overall reactions corresponding to removal of C_2H_5N from M20 and addition of C_3H_2 to M21, are suggested to locate in the B-ring side of the compound for both metabolites. The structures were relatively stable, which inhibited the formation of more informative product ions in MS/MS experiments. Despite the efforts, the exact structures of these metabolites still remain unclear. Similarly to S2 and S3, a relatively abundant (20%) metabolite of S4 was detected at the ion trace *m/z* 307 (M11b), the fragmentation of which, however, was different from the M11 metabolite of S2 and S3 (see *LC-MS/MS Characterization of the Synthesized SARM Metabolites* and Table 3). A characteristic metabolic route for S4 was deacetylation (M18), which has been earlier reported also as one of the main in vivo metabolites of S4, and being catalyzed by microsomal enzymes (Gao et al., 2006). Another main pathway was monohydroxylation (M3), which resulted in the formation of two metabolites (Fig. 1 and Table 2). In comparison with other arylpropionamide-derived SARM substrates, conjugation of monohydroxylated metabolites was to a lesser extent, as only one was detected as glucuronide-conjugate (M5), and the concentration of screened sulfonated species (M4) was too low for adequate identification with accurate mass measurements. Nitro-reduction (M7) played a more important role for S4 than what was observed for S2 or S3, although any further reactions were not observed to precede this pathway. From the minor metabolites, origin of M10 was confirmed in accurate mass measurements as demethylation reaction rather than nitro-reduction and hydroxylation, which was also supported by the product ions arising from the intact A-ring structure and by the loss of methyl group from the B-ring (Table 2).

LC-MS/MS Characterization of the Synthesized SARM Metabolites. In vitro synthesized SARM metabolites were analyzed in negative ion ESI, and in the MS full scan spectrum analysis all the compounds were detected as deprotonated species $[M\text{-}H]^-$. For the identification of the suggested SARM metabolites and their main product ions, high resolution/high accuracy measurements were carried out on an Orbitrap instrument (Tables 3 and 4). One critical parameter of the analysis was the LC-MS/MS analyzer as the ion trap technology, which is also applied in the Orbitrap, may limit the

TABLE 2

Reactions, observed $[M\text{-}H]^-$ ions, and relative abundance of the in vitro synthesized SARM metabolites

		S1		S2		S3		S4	
	Reaction	*m/z*	Rel (%)	*m/z*	Rel (%)	*m/z*	Rel (%)	*m/z*	Rel (%)
M1	Sulfonation	461	7	481	1	497	3	520	1
M2	Glucuronidation	557	7	577	13	593	3	616	0.2
M3	Monohydroxylation	397	12	417	31	433	3	456	9
M4	Monohydroxylation and sulfonation	477	1	497	1	513	1		
M5	Monohydroxylation and glucuronidation	573	2	593	8	609	1	632	0.2
M6	Dehydroxylation					401	2		
M7	Nitro-reduction			371	5	387	1	410	12
M8	Nitro-reduction and dihydroxylation			403	1				
M9	Nitro-reduction, dihydroxylation, and glucuronidation			579	1				
M10	Demethylation							426	1
M11	Dephenylation	287	44	307	23	307	73		
M11b	$C_{11}H_{10}O_5N_2F_3$							307	20
M12	Monohydroxylation of 4-cyano-3-trifluoromethyl-phenylamine	201	1						
M13	Monohydroxylation of 4-cyano/nitro-3-trifluoromethyl-phenylamine and sulfonation	281	17	301	15				
M14	Monohydroxylation of 4-cyano/nitro-3-trifluoromethyl-phenylamine and glucuronidation	377	8	397	1	397	5		
M15	Dihydroxylation of 4-cyano-3-trifluoromethyl-phenylamine and sulfonation	297	2						
M16	*N*-(4-nitro-trifluoromethyl-phenyl)-acetamide			247	1				
M17	Monohydroxylation of *N*-(4-nitro-trifluoromethyl-phenyl)-acetamide					263	6		
M18	Deacetylation							398	9
M19	Hydrolysis product					261	2		
M20	$C_{17}H_{12}O_6N_2F_3$							397	33
M21	$C_{22}H_{19}O_6N_2F_3$							478	9
X	Not-rationalized minor metabolites		0.5						6

Rel, relative abundance.

TABLE 3

MS/MS product ions obtained from in vitro synthesized SARM metabolites

Product ions indicated in italic originate from triple quadrupole studies.

	S1					S2					S3					S4				
Metabolite	$[M\text{-}H]^-$	Product Ions				$[M\text{-}H]^-$	Product Ions				$[M\text{-}H]^-$	Product Ions				$[M\text{-}H]^-$	Product Ions			
Substrate	381	269	241	185	111	401	289	261	205	*111*	417	289	261	205	127	440	289	261	205	150
M1	461	381				481	401	*261*	*205*		497	417	*261*			520	440	406		
M2	557	381	371	241	185	577	401	261	205		593	417	261	205		616	440	421	410	261
M3	397	269	241	185	127	417	289	261	205		433	289	261			456	289	261	205	166
		269	241	185	127		289	261	205	127		289	261	143			289	261		166
							289	261	205	127		289	261	205	143					
M4	477	397				497	417	*205*			513	433	*413*			520	*440*	*261*		
M5	573	397	303	241	185	593	417	289	261	205	609	433	261			632	456	261		
		397	303	241	185			417	261			433	261				456	440		
							417	289	205		433									
M6											401	*289*	*261*	*205*						
M7						371	*259*	*231*	*111*		387	349	259	201		410	259	150		
M8						403	291	263	205											
M9						579	*403*													
M10														426	289	261	136			
M11	287	269	241	185		307	289	261	205		307	289	261	205						
M11b														307	277	234	206	205		
M12	201	*181*	*161*	*154*																
M13	281	*263*	*201*	*181*		301	*221*													
M14	377	*359*	*201*		397	*221*				397	*221*	*205*								
M15	297	*217*																		
M16						247	*205*													
M17											263	*205*								
M18																398	289	261	205	
M19											261	241	218	204						
M20																397	289	261	205	165
M21																478	289	261	205	188

determination of the product ions at low *m/z* values. For this purpose, the initial screening of incubation samples was carried out in a triple quadrupole Q Trap instrument.

In addition to elemental composition, presence or absence of structure-specific ions was monitored for more detailed structure elucidation. For all the compounds within the current in vitro assay, the main metabolic reactions, excluding nitro-reduction, involved modifications in the B-ring side of the SARM structure and were, thus, leaving the A-ring core structure intact. Thus, the dissociation pathways of the main metabolites followed the earlier-reported ones by Thevis et al. (2006), that is, product ions were formed from the elimination of the B-ring moiety, subsequent loss of carbon monoxide, and from the

TABLE 4

Measured elemental composition of SARM substrates and in vitro synthesized metabolites (deprotonated species)

See Table 2 for more information.

	S1			S2			S3			S4		
Reaction	Elemental Composition $[M\text{-}H]^-$	*m/z* (exp)	Error (ppm)	Elemental Composition $[M\text{-}H]^-$	*m/z* (exp)	Error (ppm)	Elemental Composition $[M\text{-}H]^-$	*m/z* (exp)	Error (ppm)	Elemental Composition $[M\text{-}H]^-$	*m/z* (exp)	Error (ppm)
Substrate	$C_{18}H_{13}O_3N_2F_4$	381.0865	2.015	$C_{17}H_{13}O_5N_2F_4$	401.0764	2.291	$C_{17}H_{13}O_5N_2{}^{35}Cl_1F^3$	417.0469	2.228	$C_{19}H_{17}O_6N_3F_3$	440.1074	2.461
M1	$C_{18}H_{13}O_6N_2F_4S_1$	461.0429	0.959	$C_{17}H_{13}O_8N_2F_4S_1$	481.0327	0.734	$C_{17}H_{13}O_8N_2{}^{35}C\ l_1F_3S_1$	497.0035	1.415	$C_{19}H_{17}O_9N_3F_3S_1$	520.0651	3.552
M2	$C_{24}H_{21}O_6N_2F_4$	557.1183	0.951	$C_{23}H_{21}O_{11}N_2F_4$	577.1083	1.179	$C_{23}H_{21}O_{11}N_2{}^{35}Cl_1F_3$	593.0789	1.384	$C_{25}H_{25}O_{12}N_3F_3$	616.1400	2.508
M3	$C_{18}H_{13}O_4N_2F_4$	397.0812	1.620	$C_{17}H_{13}O_6N_2F_4$	417.0708	0.897	$C_{17}H_{13}O_6N_2{}^{35}Cl_1F_3$	433.0413	0.865	$C_{19}H_{17}O_7N_3F_3$	456.1026	2.715
		397.0808	0.613		417.0710	1.424		433.0407	−0.428		456.1018	1.005
					417.0709	1.161		433.0410	0.265			
M4	$C_{18}H_{13}O_7N_2F_4{}^{32}S_1$	477.0387	2.594	$C_{17}H_{13}O_9N_2F_4S_1$	497.0271	−0.345	$C_{17}H_{13}O_9N_2{}^{35}Cl_1F_3S_1$	512.9977	0.076			
M5	$C_{24}H_{21}O_{10}N_2F_4$	573.1132	1.283	$C_{23}H_{21}O_{12}N_2F_4$	593.1036	1.898	$C_{23}H_{21}O_{12}N_2{}^{35}Cl_1F_3$	609.0733	0.602	$C_{25}H_{25}O_{13}N_3F_3$	632.1356	3.465
		573.1144	2.120		593.1029	0.684		609.0729	−0.121			
					593.1038	2.118		609.0730	0.126			
M6							$C_{17}H_{13}O_4N_2{}^{35}Cl_1F_3$	401.0507	−1.038			
M7				$C_{17}H_{15}O_3N_2F_4$	371.1028	3.848	$C_{17}H_{15}O_3N_2{}^{35}Cl_1F_3$	387.0718	0.125	$C_{19}H_{19}O_4N_3F_3$	410.1324	0.296
M10										$C_{18}H_{15}O_6N_3F_3$	426.0915	1.697
M11	$C_{12}H_{10}O_3N_2F_3$	287.0647	0.936	$C_{11}H_{10}O_3N_2F_3$	307.0538	0.642	$C_{11}H_{10}O_3N_2F_3$	307.0533	−0.987			
M11b										$C_{11}H_{10}O_5N_2F_3$	307.0545	2.694
M17							$C_9H_6O_4N_2F_3$	263.0284	3.657			
M18										$C_{17}H_{15}O_5N_3F_3$	398.0966	1.803
M19	$C_{11}H_8O_1N_2F_3$	241.0587	1.724				$C_{10}H_8O_3N_2F_3$	261.0481	−0.244			
M20										$C_{17}H_{12}O_6N_2F_3$	397.0647	1.265
M21										$C_{22}H_{19}O_6N_2F_3$	478.1223	0.613

exp, experimental.

cleavage of the amide bond. The corresponding product ions were thus *m/z* 269, 241, and 185 for cyano-substituted S1 and analogously *m/z* 289, 261, and 205 for nitro-substituted S2, S3, and S4 (Table 3). The data obtained from high resolution-high accuracy mass analysis supported the identical elemental composition also for the product ions resulting from the in vitro synthesized metabolites (data not shown).

In fragmentation the charge was not prominently only on the A-ring side residue, which provided information also on the B-ring counterpart, such as *m/z* 111 for S1 and *m/z* 127 for its B-ring monohydroxylated metabolite (M3). With this respect, from three monohydroxylated metabolites of compounds S2 and S3, two are suggested to bear the monohydroxyl function in the B-ring structure, as they cleave fragments *m/z* 127 and 143 (Table 3). From the MS/MS-spectrum of the first-eluting metabolite M3, these fragments are missing, revealing the ether-linked carbon as the potential site of hydroxylation, which has been suggested for S2 by Wu et al. (2006).

An interesting MS behavior was observed in the CID spectra of precursor ions of *O*-dephenylated metabolites M11, corresponding *m/z* 287 for S1 and *m/z* 307 for S2, S3, and S4 (Fig. 2). With compounds S1, S2, and S3, the fragmentation followed the above-mentioned pathway, whereas for the S4-metabolite M11b exceptional fragments at *m/z* 277 (determined elemental composition $C_{10}H_8O_4N_2F_3$; error from the theoretical 2.497 ppm), *m/z* 234 ($C_9H_7O_3N_1F_3$; 4.339 ppm), and *m/z* 206 ($C_7H_3O_3N_1F_3$; 5.367 ppm) were detected instead. Elemental composition of this peak was equivalent with *O*-dephenylated metabolites of S2 and S3 ($C_{11}H_{10}O_5N_2F_3$) with good fit of accurate mass (2.563 ppm). Product ion *m/z* 205 ($C_7H_4O_2N_2F_3$), originating from an intact nitro-substituted A-ring, was observed in the MS/MS spectrum, revealing the B-ring side of the molecule as the site of modifications. This is probably due to gas-phase deacetylation and the acidic hydrogen located at the amide residue in *para*-position of the B-ring. The additional ionization site can lead to a charge-driven dissociation different from halogen-substituted compounds S2 and S3. Similar behavior was reported earlier with diuretic agents (e.g., furosemide) (Thevis et al., 2003).

Metabolites originating from the hydrolysis of amide-bond and A-ring hydroxylation (M12-M15) resulted in the formation of the low-mass fragments (*m/z* < 200), which were outside the range of Orbitrap. The analysis by the triple quadrupole instrument, however, enabled the structural characterization of the metabolites (Table 3). Characteristic ions at *m/z* 201 and *m/z* 221, originating from a monohydroxylated A-ring structure, were thus detected for cyano-substituted S1-metabolites and nitro-substituted metabolites of S2 and S3, respectively.

Sulfonated and glucuronide-conjugated SARM metabolites were detected as deprotonated molecules $[M\text{-}H]^-$, and the charge remained preferably in the aglycone and asulfate side. Thus, CID in product ion scan mode resulted in ions indicative only of the loss of an intact glucuronide or sulfate moiety and structure-specific fragments of aglycones (Table 3). In the initial screening of in vitro assay samples, neutral loss scans of glucuronide (176 amu) and sulfate (80 amu) moieties were thus the most effective procedures to target group-specific phase-II reactions by the triple-quadrupole instrument.

Discussion

Due to their advantageous anabolic properties and reduced side-effects, selective androgen receptor modulators are a prominent new group of compounds for being misused in sports and, therefore, although not currently being marketed, knowledge of their metabolic and analytical behavior is of the utmost importance in preventive doping control. To overcome the problems connected to ethically and practically complicated in vivo experiments, especially in the case of

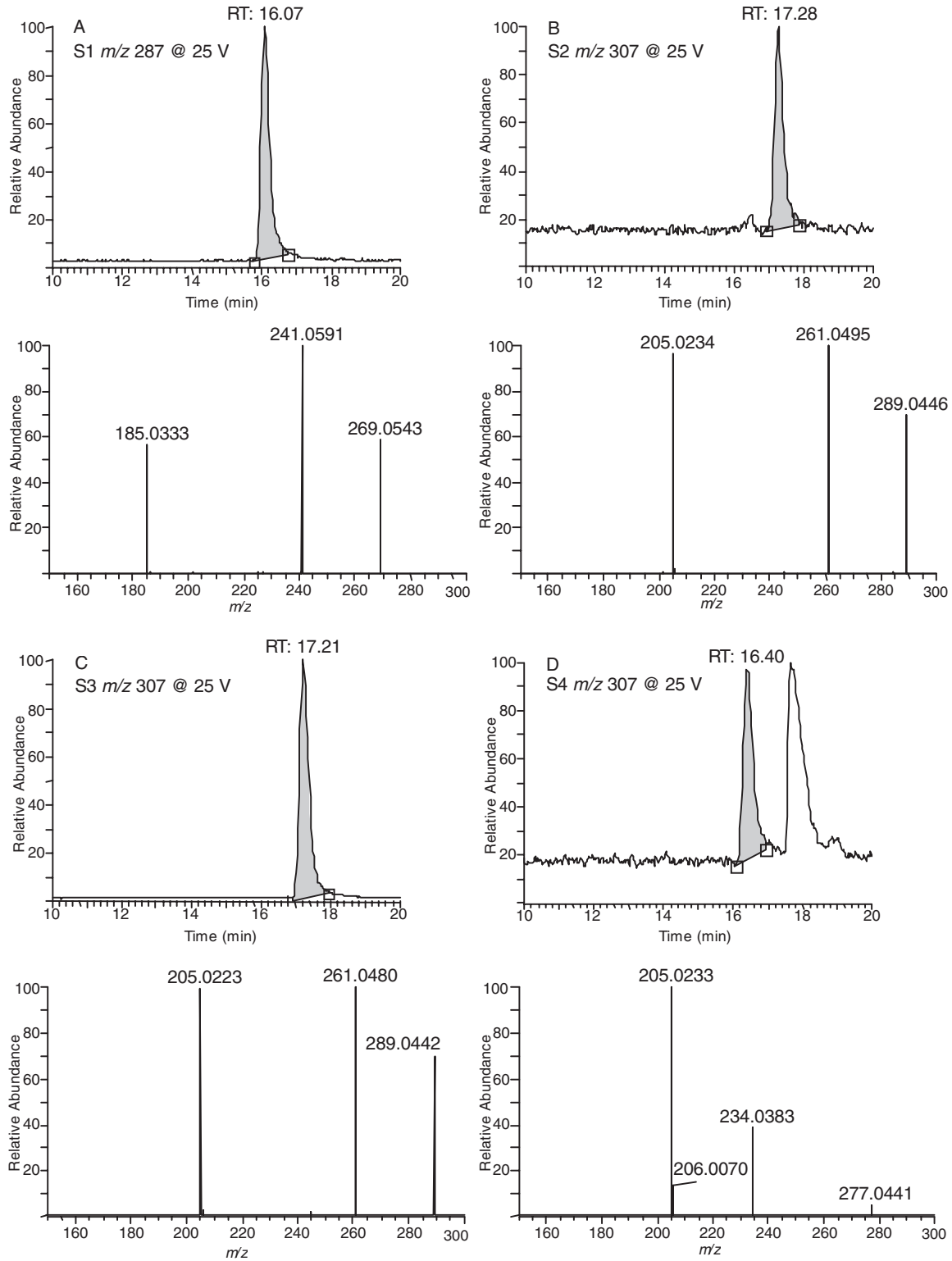

FIG. 2. Extracted ion chromatograms of *m/z* 287 and *m/z* 307 and spectra at collision offset voltage of 25 V from (A) S1, (B) S2, (C) S3, and (D) S4. RT, retention time.

drug candidates without completed pharmacological data, an enzyme-assisted in vitro assay was developed to predict the phase-I and phase-II metabolic reactions of aryl-propionamide-derived SARM. This approach offered a practical pathway for the rapid production of metabolites in amounts needed (e.g., in the build-up of an analytical method).

In this study, subsequent phase-I and phase-II metabolic reactions were successfully combined for preventive doping control purposes in one in vitro assay in order to examine the metabolic reactions, main metabolites, and LC-MS/MS behavior of aryl-propionamide-derived SARM. To serve as a potential default assay for the in vitro metabolite production of a new doping substance, the procedure was simple and straightforward and targeted to produce an extensive selection of SARM metabolites. Enzymes from microsomal and S9 fractions of

human liver were purchased from commercially available sources and applied to catalyze the reactions from which the main routes of phase-I modifications involved the hydrolysis of ether linkage (i.e., *O*-dephenylation) monohydroxylation and hydrolytic cleavage of the amide bond (Fig. 3). Reduction was observed for those substrates having an A-ring nitro-group in the structure, and it was found most extensive for S4. Two of the target compounds (S2 and S4) were investigated in detail earlier (Gao et al., 2006; Wu et al., 2006) in terms of phase-I and phase-II metabolism, and results of the present study substantiated and complemented these findings with two additional substrates (S1 and S3). A significant difference between recent publications and the present work was the observation of the metabolite arising from *O*-dephenylation, which was not reported before but represents a metabolic product that possesses great potential as a target analyte for doping control purposes. Two options of its formation are illustrated in Fig. 4, which are in accordance with metabolic reactions proposed for other substances such as the nontricyclic antidepressant nefazodone (Kalgutkar et al., 2005). In particular, the fact that M11 was most abundant in case of the chlorinated substance S3 might provide a hint and mechanistic insight. Further experiments demonstrated that the formation of M11 for S1, S2, and S3, as well as M11b for S4, is NADPH-independent, that is, not mediated by CYP450 enzymes but dependent on the presence of enzymes. Hence, the option presented as route B in Fig. 4 seems more likely. Based on a theoretically possible structure, including alkylation of the amide bond and introduction of a deuterated methyl residue, a synthesis experiment was conducted to clarify the composition of M11b. However, no conclusive result was obtained to justify a scientifically sound suggestion for this metabolic product, the presence of which should be confirmed in future in vivo experiments in humans.

Within the current set of selected aryl-propionamide-derived SARM (Table 1), the structural modifications were located in the A-ring (cyano-function or nitro-function) and in the B-ring *para*-substitution (chlorine, fluorine, or acetylamide). With respect to A-ring modifications and in comparison between S1 and S2, the effect of nitro-function to increase metabolic activity was detected, as a higher number of metabolites was recorded for S2, and most of those additional metabolites (M7, M8, and M9) involved nitro-reduction. The effect of cyano- or nitro-function as A-ring substitute was not observed as the major factor on the amide hydrolysis, but merely A-ring hydroxylation, as all the metabolites that showed hydrolytic activity of the amide bond were also hydroxylated. For S2, three monohydroxylated metabolites (M3) were detected, but based on the MS/MS studies for S1, the hydroxylation of the ether-linked carbon either did not occur or the activity was significantly lower than for S2, and as a result only two monohydroxylated metabolites were observed.

Halogen substitution is often used to block metabolism or to deactivate ring systems (Birnbaum, 1985), and thus higher electronegativity in the B-ring substituent could be suggested to result (e.g., into lower hydroxylation activity of the B-ring). Within the test set the highest relative hydroxylation activity was observed for fluorine-substituted S2 and the lowest for acetylamide-substituted S4, which is, however, quite opposite to the hypothesis, although due to extensive *O*-dephenylation, hydrolysis, and deacetylation reactions (S4), a true comparison between hydroxylation activities of these compounds is complicated. Hydrolysis activity did not follow a clear electronegativity-dependent pattern either, although the total relative abundance of hydrolyzed metabolites was clearly lower for S2 than for S3 and S4 with less electronegative substituents (Table 2).

From the main conjugation reactions, the sulfotransferase system is generally considered a high-affinity, low-capacity pathway and the UDP-glucuronosyltransferase system a low-affinity, high-capacity pathway (Burchell and Coughtrie, 1997), and therefore the optimal synthesis conditions are probably different for these two systems. Features such as product and substrate inhibition have been reported especially characteristic for sulfotransferases (Chapman et al., 2004; Gamage et al., 2006), and these parameters should be optimized in detail when the interest of the assay is in the synthesis of a specific metabolite. In our in vitro assay conditions and with an extensive incubation time, both types of conjugates were formed, and the same SARM metabolites were substrates for both systems, although differences between relative abundance of the sulfonated metabolites and the corresponding glucuronide conjugates were not significant. Phase-I hydroxylation reactions offer prominent sites for phase-II reactions, but as the substrates themselves were also directly glucuronidated and sulfonated, the suggested conjugation site is hydroxyl group attached to the chiral center of the compound.

In an earlier in vivo administration study (Wu et al., 2006) of S2 in rats, 37 phase-I and phase-II metabolites were identified in the urine, the main phase-I modifications arising from amide hydrolysis, A-ring nitro-reduction, and B-ring hydroxylation, which is well in agreement with the current assay. Pharmacokinetic studies of S4 in rats (Kearbey et al., 2004) determined the lack of parent drug in the urine, thus suggesting extensive metabolism, and the more recent in vitro metabolism studies with several enzyme preparations revealed deacetylation, amide hydrolysis, A-ring nitro-reduction, and hydroxylation of aromatic rings as the major phase-I pathways in humans (Gao et al., 2006). In that study, microsomal enzymes were observed to contribute to deacetylation reaction, cytosolic enzymes to hydrolysis, and the role of CYP3A4 enzymes as one of the major phase-I enzymes to catalyze deacetylation, hydrolysis, and oxidative reactions. In the current in vitro assay, the combination of crude S9 fraction and pure microsomal fraction of enzymes resulted in formation of all these major metabolites and an additional two major metabolites, the exact structures of which could not be confirmed within this study.

Negative ion ESI was applied in the ionization of the in vitro synthesized SARM metabolites, which all were detected as deprotonated species $[M\text{-}H]^-$. Without the application of quantitative reference material, the determination of the relative abundance of SARM metabolites potentially includes a source of error. In their earlier work, Wu et al. (2006) demonstrated the less ionization efficiency for those metabolites containing only a single phenyl ring, especially for lipophilic metabolites. Although this issue is relevant from a pharmacological point of view, the focus of this study was to monitor and characterize the main metabolites of aryl-propionamide-derived SARM and to consider the analytical approach for doping control purposes. Therefore, the LC-ESI-MS and MS/MS methods were applicable despite these limitations.

In doping control, the analysis should be targeted in the most representative metabolites, in which the challenge is to predict the metabolic fate of a new compound. The observed metabolic modifications of aryl-propionamide-derived SARM involved mainly the B-ring structure. The main metabolites were still extremely nonpolar, and thus the earlier-reported solid-phase extraction method (Thevis et al., 2006) may be applied in the sample preparation, especially if the hydrolysis step is added to the procedure. To ensure the detection of the total fraction of metabolites, enzyme preparation with both glucuronidase and sulfatase activities should be applied. Collision-induced dissociation of the main metabolites resulted in the product ions originating from the A-ring side of the compound, that is, from elimination of the B-ring moiety, subsequent loss of carbon monoxide, and from the cleavage of the amide bond, producing characteristic fragment ions *m/z* 269, 241, and 185 for S1 and *m/z* 289, 261, and 205

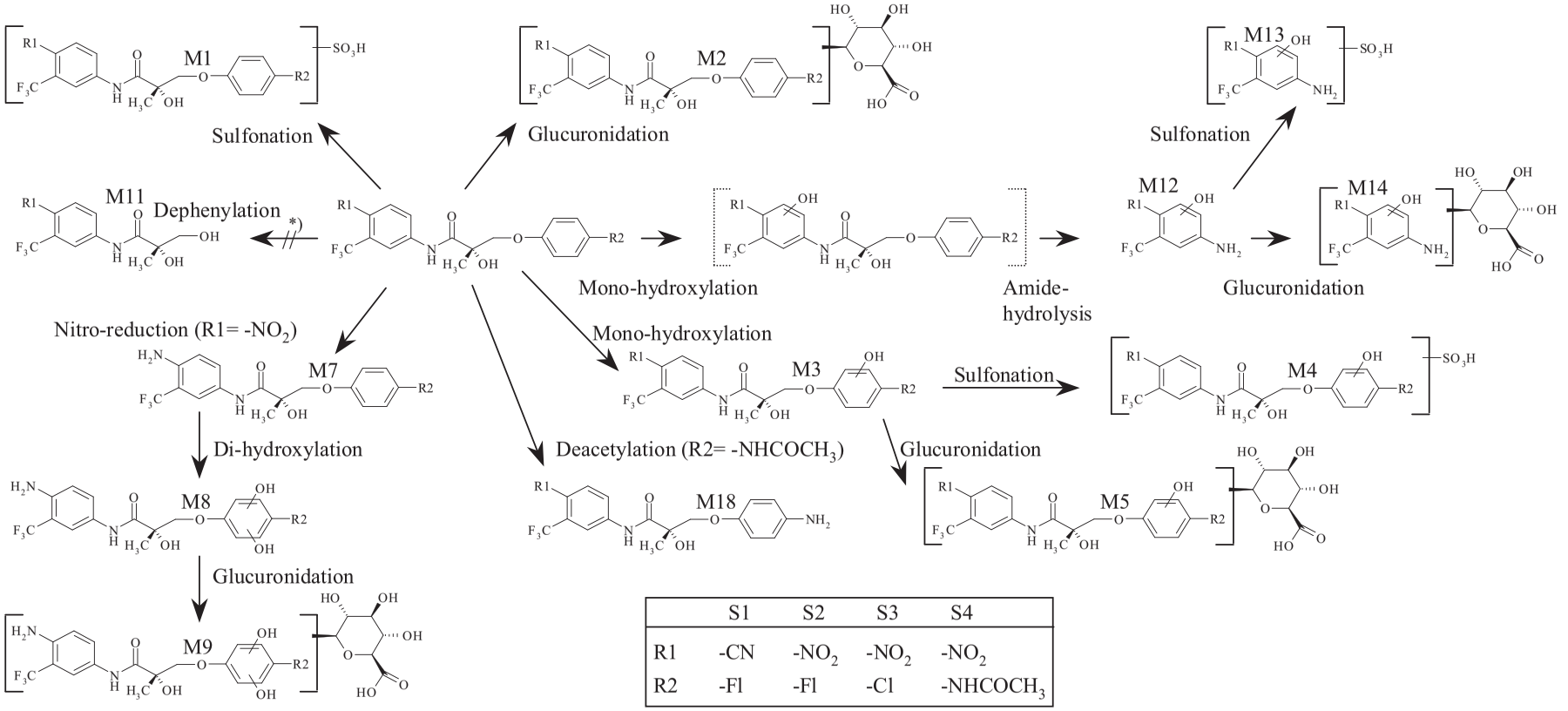

	S1	S2	S3	S4
R1	-CN	$-NO_2$	$-NO_2$	$-NO_2$
R2	-Fl	-Fl	-Cl	$-NHCOCH_3$

*) potentially involving several transition states

FIG. 3. Suggested main metabolic routes of aryl-propionamide-derived SARM within the study. See Tables 1 and 2 for more information.

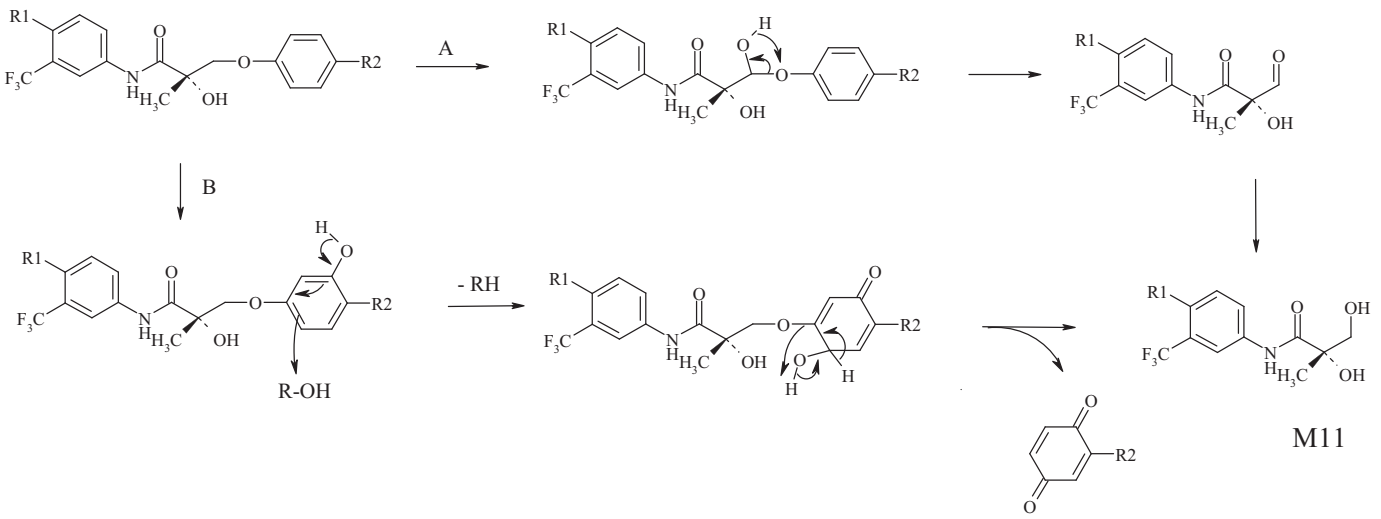

FIG. 4. Proposed mechanisms for the *O*-dephenylation of selected SARM. Route A is initiated by the hydroxylation of the carbon adjacent to the ether oxygen followed by the generation of an aldehyde upon release of the phenyl residue. Subsequent reduction of the aldehyde gives rise to the proposed structure of M11. Alternatively, the formation of M11 can be triggered by a hydroxylation of the phenyl residue *ortho*-positioned to the substituent R2 (route B). Further hydroxylation favors the release of a 2-substituted 1,4-benzoquinone also yielding M11.

for S2, S3, and S4. SARM in general are an earlier-claimed flexible group of compounds for structural modifications (Brown 2004), but with clinically promising aryl-propionamide-derived compounds the A-ring core structure with 3-trifluoromethyl-4-nitro substitution seems like the one possessing the most advantageous pharmacological and pharmacokinetic properties. The main metabolic modifications occur in the B-ring side of the structure and cleave structure-specific fragments originating from the A-ring side, and these product ions are also the targets of the routine doping control screening. In addition to targeted MS/MS analysis of the metabolites of the most prominent drug candidates, S2 and S4, a precursor ion scan of these structure-specific ions would allow the detection of structurally related compounds in routine doping control. The reported maximum daily doses of aryl-propionamide-derived SARM are 3 mg (http://www.salesandmarketingnetwork.com/news_release.php?ID=2015328), which is a challenge to precursor ion scan mode, the sensitivity being, however, strongly dependent on the ionization efficiency of each metabolite.

Targeted analysis to relevant metabolites of banned substances exhibits a challenge to doping control laboratories, especially with compounds lacking a clinical approval to enter the market. In the current work, an in vitro assay employing human liver enzymes was found as a suitable pathway to synthesize metabolites of aryl-propionamide-derived SARM, which can be applied to method development in routine doping control analysis. Representatives of the selected class of SARMs have completed phase-II clinical trials and may enter the pharmaceutical market in the near future; however, they are officially considered relevant for sports drug-testing as early as January 2008, because the World Anti-Doping Agency has added those therapeutics to the list of prohibited compounds. Hence, the rapid preparation of possible targets for doping control purposes has become necessary and was accomplished using the applied in vitro approach. After clinical approval of these drug candidates, administration study urine samples and chemically synthesized reference substances of metabolites will be the first choice to identify surreptitiously applied SARMs in sports drug-testing. But the fast nature of the employed in vitro assay yielding metabolic products that simulate to an acceptable extent the human metabolism serves the purpose for method development and target compound screening.

References

Bhasin S and Bremner WJ (1997) Clinical review 85: Emerging issues in androgen replacement therapy. *J Clin Endocrinol Metab* **82:**3–8.

Birnbaum LS (1985) The role of structure in disposition of halogenated aromatic xenobiotics. *Environ Health Perspect* **61:**11–20.

Bohl CE, Chang C, Mohler ML, Chen J, Miller DD, Swaan P, and Dalton JT (2004) A ligand-based approach to identify quantitative structure-activity relationships for the androgen receptor. *J Med Chem* **47:**3765–3776.

Brown TR (2004) Nonsteroidal selective androgen receptor modulators (SARMs): designer androgens with flexible structures provide clinical promise. *Endocrinology* **145:**5417–5419.

Burchell B and Coughtrie MWH (1997) Genetic and environmental factors associated with variation of human xenobiotic glucuronidation and sulfation. *Environ Health Perspect* **105:** 739–747.

Catlin DH, Ahrens BD, and Kucherova Y (2002) Detection of norbolethone, an anabolic steroid never marketed, in athletes' urine. *Rapid Commun Mass Spectrom* **16:**1273–1275.

Catlin DH, Sekera MH, Ahrens BD, Starcevic B, Chang YC, and Hatton CK (2004) Tetrahydrogestrinone: discovery, synthesis, and detection in urine. *Rapid Commun Mass Spectrom* **18:**1245–1249.

Chapman E, Best MD, Hanson SR, and Wong CH (2004) Sulfotransferases: structure, mechanism, biological activity, inhibition, and synthetic utility. *Angew Chem Int Ed Engl* **43:**3526–3548.

Chen J, Kim J, and Dalton JT (2005a) Discovery and therapeutic promise of selective androgen receptor modulators. *Mol Interv* **5:**173–188.

Chen J, Hwang DJ, Chung K, Bohl CE, Fisher SJ, Miller DD, and Dalton JT (2005b) In vitro and in vivo structure-activity relationships of novel androgen receptor ligands with multiple substituents in the B-ring. *Endocrinology* **146:**5444–5454.

Gamage N, Barnett A, Hempel N, Duggleby RG, Windmill KF, Martin JL, and McManus ME (2006) Human sulfotransferases and their role in chemical metabolism. *Toxicol Sci* **90**:5–22.

Gao W and Dalton JT (2007) Expanding the therapeutic use of androgens via selective androgen receptor modulators (SARMs). *Drug Discov Today* **12:**241–248.

Gao W, Reiser PJ, Coss CC, Phelps MA, Kearbey JD, Miller DD, and Dalton JT (2005) Selective androgen receptor modulator treatment improves muscle strength and body composition and prevents bone loss in orchidectomized rats. *Endocrinology* **146:**4887–4897.

Gao W, Wu Z, Bohl CE, Yang J, Miller DD, and Dalton JT (2006) Characterization of the in vitro metabolism of selective androgen receptor modulator using human, rat, and dog liver enzyme preparations. *Drug Metab Dispos* **34:**243–253.

Kalgutkar AS, Vaz ADN, Lame ME, Henne KR, Soglia J, Zhao SX, Abramov YA, Lombardo F, Collin C, Hendsch ZS, et al. (2005) Bioactivation of the nontricyclic antidepressant nefazodone to a reactive quinone-imine species in human liver microsomes and recombinant cytochrome P450 3A4. *Drug Metab Dispos* **33:**243–253.

Kearbey JD, Wu D, Gao W, Miller DD, and Dalton JT (2004) Pharmacokinetics of *S*-3-(4-acetylamino-phenoxy)-2-hydroxy-2-methyl-N-(4-nitro-trifluoromethyl-phenyl)-propionamide in rats, a non-steroidal selective androgen receptor modulator. *Xenobiotica* **34:**273–280.

Kirkovsky L, Mukherjee A, Yin D, Dalton JT, and Miller DD (2000) Chiral nonsteroidal affinity ligands for the androgen receptor. 1. Bicalutamide analogues bearing electrophilic groups in the B aromatic ring. *J Med Chem* **43:**581–590.

Marhefka CA, Gao W, Chung K, Kim J, He Y, Yin D, Bohl C, Dalton JT, and Miller DD (2004) Design, synthesis, and biological characterization of metabolically stable selective androgen receptor modulators. *J Med Chem* **47:**993–998.

Mohler ML, Nair VA, Hwang DJ, Rakov IM, Patil R, and Miller DD (2005) Nonsteroidal tissue selective androgen receptor modulators: a promising class of clinical candidates. *Expert Opin Ther Patents* **15:**1565–1585.

Negro-Vilar A (1999) Selective androgen receptor modulators (SARMs): a novel approach to androgen therapy for the new millenium. *J Clin Endocrinol Metab* **84:**3459–3462.

Sekera MH, Ahrens BD, Chang YC, Starcevic B, Georgakopoulos C, Catlin DH (2005) Another

design steroid: discovery, synthesis, and detection of 'madol' in urine. *Rapid Commun Mass Spectrom* **19:**781–784.

Thevis M, Kamber M, and Schänzer W (2006) Screening for metabolically stable arylpropionamide-derived selective androgen receptor modulators for doping control purposes. *Rapid Commun Mass Spectrom* **20:**870–876.

Thevis M and Schänzer W (2007) Emerging drugs—potential misuse in sport and doping control detection strategies. *Mini Rev Med Chem* **7:**531–537.

Thevis M, Schänzer W, and Schmickler H (2003) Effect of the location of hydrogen abstraction on the fragmentation of diuretics in negative electrospray ionization mass spectrometry. *J Am Soc Mass Spectrom* **14:**658–670.

Tucker H and Chesterson GJ (1988) Resolution of the nonsteroidal antiandrogen 4′-cyano-3-[(4-fluorophenyl)sulfonyl]-2-hydroxy-2-methyl-3′-(trifluoromethyl)-propionanilide and the determination of the absolute configuration of the active enantiomer. *J Med Chem* **31:**885–887.

Tucker H, Crook JW, and Chesterson GJ (1988) Nonsteroidal antiandrogens. Synthesis and structure-activity relationships of 3-substituted derivatives of 2-hydroxypropionanilides. *J Med Chem* **31:**954–959.

Wu D, Wu Z, Yang J, Nair VA, Miller DD, and Dalton JT (2006) Pharmacokinetics and metabolism of selective androgen receptor modulator in rats: implication of molecular properties and intensive metabolic profile to investigate ideal pharmacokinetic characteristics of a propanamide in preclinical study. *Drug Metab Dispos* **34:**483–494.

Address correspondence to: Dr. Mario Thevis, Institute of Biochemistry—Center for Preventive Doping Research, German Sports University Cologne, Carl-Diem Weg 6, 50933 Cologne, Germany. E-mail: m.thevis@biochem.dshs–koeln.de